IOPscience iopscience.iop.org

Home Search Collections Journals About Contact us My IOPscience

A superconducting nanowire single photon detector on lithium niobate

This content has been downloaded from IOPscience. Please scroll down to see the full text.

2012 Nanotechnology 23 505201

(http://iopscience.iop.org/0957-4484/23/50/505201)

View the table of contents for this issue, or go to the journal homepage for more

Download details:

IP Address: 131.152.109.100

This content was downloaded on 16/05/2014 at 12:24

Please note that terms and conditions apply.

Nanotechnology 23 (2012) 505201 (6pp) doi:10.1088/0957-4484/23/50/505201

A superconducting nanowire single photon detector on lithium niobate

M G Tanner[1], L San Emeterio Alvarez[2], W Jiang[2,3], R J Warburton[4], Z H Barber[2] and R H Hadfield[1]

[1] Scottish Universities Physics Alliance and School of Engineering and Physical Sciences, Heriot-Watt University, Edinburgh EH14 4AS, UK
[2] Department of Materials Science and Metallurgy, University of Cambridge, Pembroke Street, Cambridge CB2 3QZ, UK
[3] State Key Laboratory for Manufacturing Systems Engineering, Xi'an Jiaotong University, Xi'an 710049, People's Republic of China
[4] Department of Physics, University of Basel, Klingelbergstrasse 82, CH-4056 Basel, Switzerland

E-mail: M.Tanner@hw.ac.uk

Received 5 July 2012, in final form 2 October 2012
Published 26 November 2012
Online at stacks.iop.org/Nano/23/505201

Abstract
Superconducting nanowire single photon detectors (SNSPDs) are a key enabling technology for optical quantum information science. In this paper we demonstrate a SNSPD fabricated on lithium niobate, an important material for high speed integrated photonic circuits. We report a system detection efficiency of 0.15% at a 1 kHz dark count rate with a maximum of ∼1% close to the critical current at 1550 nm wavelength for a parallel wire SNSPD with front side illumination. There is clear scope for improving on this performance with further materials optimization. Detector integration with a lithium niobate optical waveguide is simulated, demonstrating the potential for high single photon detection efficiency in an integrated quantum optic circuit.

(Some figures may appear in colour only in the online journal)

Fast, efficient, low noise single photon detection is required if photons are to be used as the qubit for quantum computation [1, 2]. Superconducting nanowire single photon detectors (SNSPDs) offer excellent timing resolution, as low as 29 ps full width half maximum (FWHM) [3], whilst operating over a wide wavelength range (covering common single photon source emission and standard telecommunications wavelengths) with a low dark count rate (DCR) [4]. These properties have led to the use of SNSPDs for waveguide quantum optics experiments including characterization of correlated photon pair sources [5–7] and quantum optic circuit elements [8, 9].

Development of scalable quantum computing architectures requires on-chip integration of *all* the demonstrated circuit elements, including detectors. SNSPDs are appropriate for this endeavour due to their relatively simple architecture, as opposed to competing technologies such as single photon avalanche diodes (SPADs) [2]. Integration of SNSPDs with optical waveguides has been recently demonstrated on sapphire [10], silicon [11] and gallium arsenide [12] based substrates. The use of lithium niobate ($LiNbO_3$ = LN) as a substrate for SNSPDs has not yet been explored. LN is a widely used material in low loss, high speed telecom lightwave circuits [13]. The usefulness of LN waveguide elements in the arena of quantum information science has recently been demonstrated [5, 7, 8]. Fast path and polarization manipulation has been shown in waveguides at telecom wavelengths [8]. Periodically poled lithium niobate (PPLN) [7] and lithium tantalate (PPLT) [5] waveguide photon pair sources have been demonstrated. The integration of SNSPDs on chip is thus a crucial future target. In this paper we demonstrate the first step on this path—the realization of a SNSPD on a LN substrate.

SNSPDs require a thin film (∼10 nm or less) of a superconducting material such as niobium nitride (NbN) to be grown on the substrate, followed by nanoscale patterning of the nanowire detector. Growth and fabrication of SNSPDs is best achieved on substrates for which lattice matching and/or high temperature growth can lead to epitaxial or high quality crystalline films, e.g. MgO [14, 15] and sapphire

 © 2012 IOP Publishing Ltd Printed in the UK & the USA

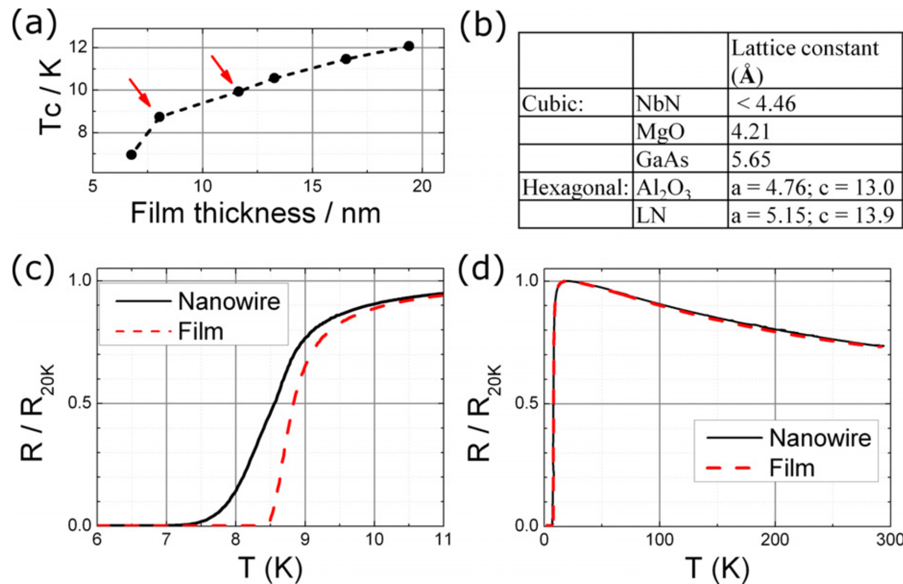

		Lattice constant (Å)
Cubic:	NbN	< 4.46
	MgO	4.21
	GaAs	5.65
Hexagonal:	Al_2O_3	a = 4.76; c = 13.0
	LN	a = 5.15; c = 13.9

Figure 1. (a) Critical temperature of NbN films grown on LN at 200 °C. Devices were fabricated from the films marked with arrows. (b) Table of lattice constants. (c), (d) Normalized resistance of the 8 nm thick film and nanopatterned device with temperature; both were biased at 1% of their I_c at 2.5 K.

(Al_2O_3) [16]. Figure 1(b) Shows lattice parameters for NbN and relevant substrates. Note that MgO offers perfect cube-on-cube lattice matching to NbN and hence high quality epitaxial growth can be achieved, even at a relatively low growth temperature. Conversely, sapphire has a hexagonal lattice (as does LN), and does not lead to obvious epitaxial lattice matching. For example, NbN films grown at high temperature (750 °C) on *r*-plane sapphire have been shown to have a nanocrystalline structure [17].

Recent progress has been made on other substrates including fabricating meander SNSPDs on silicon [18, 19] and gallium arsenide [20] based materials. Here we show successful growth and fabrication of a SNSPD on LN with reasonable device properties as a proof of principle demonstration of the potential for integration with quantum optic circuits. Device coupling to a waveguide architecture is discussed, including the expected high absorption probability achievable in this arrangement.

Sputtering of NbN thin films was optimized by varying the gas mixture, pressure and sputtering power at relatively low temperatures to avoid the possibility of unwanted annealing of photonic structures [21] in future devices. Deposition was carried out at a sample temperature of 200 °C, a total gas pressure of 1.6 Pa (Ar + 30%N_2) and DC reactive magnetron sputtering power of 150 W (target area 35 mm × 55 mm). Film thickness was measured via low angle x-ray diffraction, allowing the dependence of T_c on film thickness to be plotted in figure 1(a).

The film used for the main device discussed in this paper was 8 nm thick (left-hand arrow in figure 1(a)), with a critical temperature (T_c) of approximately 8.5 K, defined as the temperature at which the resistance reaches zero. In comparison optimized (high temperature) growth on sapphire achieves T_c of >11 K for the same film thickness in this sputtering system. The nanowires were patterned through electron beam exposure of PMMA, a positive e-beam resist, and reactive ion etching of the film.

The 8 nm film was analysed in a closed cycle refrigerator after patterning of test structures (∼5 μm in width, which can be assumed to have properties close to that of unpatterned, or 'bulk film') and nanoscale device structures (∼70 nm width). Figures 1(c) and (d) show the normalized resistance versus temperature of each. Compared to the test structure (with approximately bulk film properties), the nanopatterned structure has a reduced T_c of 7.0 K. The width of transition, defined as the change in temperature in which the resistance falls from 90% to 10% of its 20 K value, has increased from 1.58 to 1.97 K. The residual resistance ratio ($R_{300\text{ K}}/R_{20\text{ K}}$) remains at 0.74 for both the film and device structure. The lower T_c and increased transition width of the nanostructured features, as compared to the bulk film and coarse test structures, suggest that low temperature (200 °C) NbN film growth leads to less uniform nanoscale tracks. We suggest that this is due to a film structure that is more susceptible to processing and etching damage than that observed for higher deposition temperatures [17, 23] and high quality epitaxial film growth [22].

For comparison, table 1 describes properties of NbN films on other substrates. While the available literature includes results from a large number of groups, details included in the table are chosen from references where clear explanations are given of the definitions used to determine the quoted parameters and where a range of film thicknesses were tested. In this case the quoted parameters may not be the 'best' ever published and the list of substrates is not exhaustive, but they provide a useful comparison to the properties of films on LN described in this work.

It is clear that very high quality epitaxial film growth achieved through exact lattice matching (on MgO), or high temperature growth (for example on sapphire), led to films

Table 1. Transport properties of NbN thin films grown on a variety of substrates. Values are either quoted directly, read from figures or calculated from data provided within the referenced works except where noted. Film thickness (t), patterned width (w), substrate growth temperature (T_{growth}), critical temperature (T_c), definition of T_c (T_c details), transition width for 90–10% resistance (ΔT_c), residual resistivity ratio (RRR) and critical current density (J_c) are stated where available for comparison.

Substrate	t (nm)	w (nm)	T_{growth}(°C)	T_c (K)	T_c details	ΔT_c (K)	RRR	J_c (4.2 K) (MA cm^{-2})	J_c (2.5 K) (MA cm^{-2})
MgO	3.9	80	Ambient[a]	10.8	50% R_{20K}			5.9	
Reference [22]	3.9	200	Ambient	11.0	50% $R_{20\ K}$			6.0	
	4.2	80	Ambient	11.1	50% $R_{20\ K}$	1.4[b]	0.91[b]		
	7	Film	Ambient	13.3	50% $R_{20\ K}$				
	10	Film	Ambient	14.1	50% $R_{20\ K}$				
Al_2O_3	4.3	Film	750	12.44	Fit[c]		0.856	6.4[d]	7.0[d]
(Sapphire)	5.6	Film	750	12.99	Fit		0.922	7.4	8.0
Reference [17, 23]	8	Film	750	13.99	Fit		0.979	10.4	11.1
	11.7	Film	750	15.2	Fit		0.98	12.4	13.1
GaAs	4.5	Film	400	9.2	50% $R_{20\ K}$	1.7			
Reference [24]				8.1	0% $R_{20\ K}$				
	5.5	Film	400	10.3	50% $R_{20\ K}$	1.65	0.74		
	10	Film	400	12.4	50% $R_{20\ K}$	0.8	0.76		
				12.0	0% $R_{20\ K}$				
$LiNbO_3$	8	5000	200	8.8	50% $R_{20\ K}$	1.58	0.74		1.04
				8.5	0% $R_{20\ K}$				
	8	70 (x4)	200	8.6	50% $R_{20\ K}$	1.97	0.74		0.58
				7.0	0% $R_{20\ K}$				
	8	Film	360	11.2	0%$R_{20\ K}$				

[a] Quoted as ambient temperature [22], but there may be radiative substrate heating from the power input to the target.
[b] Measured by authors with a nanowire device matching those described in [14].
[c] Calculated T_c from theoretical fit to $R(T)$ curve near T_c [17].
[d] Calculated for $T = 4.2$ K and 2.5 K for comparison with other substrates, J_c at 0 K values are quoted in [17].

with notably higher T_c and J_c with RRR closer to 1, even for ∼4 nm thin films. It is interesting to observe that patterning of 3.9 nm thick films on MgO to small feature sizes (80 nm) appeared to have little detrimental effect on the electrical characteristics, unlike the described results on LN. Characteristics for films grown on a substrate with poor lattice matching, such as GaAs at a substrate temperature of 400 °C, are more comparable to those on LN at low temperature. The RRR is similar, and the width of the superconducting transition for the 8 nm LN films is similar to that of the 5.5 nm film on GaAs. However, the critical temperature for the LN films grown at 200 °C are slightly lower.

While the film growth results on LN do not compare favourably in table 1 it is important to note that the majority of growth was limited to a substrate temperature of 200 °C (compared to 750 °C on Al_2O_3 and 400 °C on GaAs) for compatibility with hydrogen implanted waveguides. Growth on LN at 360 °C had much improved T_c, comparing well to that of GaAs. Growth on LN substrates could be considered to be at a similar stage of development to the growth on GaAs described in table 1. However, superconductivity is achieved for 70 nm width nanowires patterned on an 8 nm thick NbN film on LN suitable for single photon detection even after film growth at low temperature.

The SNSPD reported in detail in this paper is a parallel wire design, sometimes referred to as a cascade switching [25, 26] or superconducting nanowire avalanche detector (SNAP) [27]. In this design the width of each nanowire can be reduced compared to single wire SNSPDs, while maintaining a high critical current and therefore a good signal to noise ratio for the output pulse. Four straight wires are patterned in parallel with 70 nm width, 140 nm pitch and 10 μm length. The four wires rejoin at the end of the section, which is then repeated a total of 17 times in series as shown in figure 2(a). The total length of 70 nm wide nanowire is 680 μm: uniformity along the length is critical to device operation [28, 29]. The detector fills a 10 μm × 10 μm area to allow efficient front side fibre coupling [19]. An additional broad meander (1 μm line width) is patterned in series to increase the kinetic inductance of the device to aid the cascade process [26, 27, 30].

The device is biased close to its critical current ($I_{bias} < I_c$, expected to be four times that of an individual nanowire of the same dimensions as the four nanowires arranged in parallel in each section of this device [26, 27]). As such, any nanowire element is biased close to its critical current density. When a photon is absorbed by a nanowire a hotspot forms and the current is diverted. This increases the current in the neighbouring wires in the same device section, causing them to cascade to the resistive state. The entire current is then shunted out of the device giving a measurable output pulse.

Detailed nano-optical studies presented in this paper were performed at 3.5 K in a closed cycle refrigerator with optic fibre feedthroughs for device illumination. The SNSPD was characterized using an *in situ* miniature confocal microscope arrangement described elsewhere [28] with ∼1.3 μm FWHM spot size at $\lambda = 1550$ nm. Vibration isolation has been optimized with a new configuration: the confocal microscope is mounted on a stand-off stage linked to the cold head by flexible copper braids.

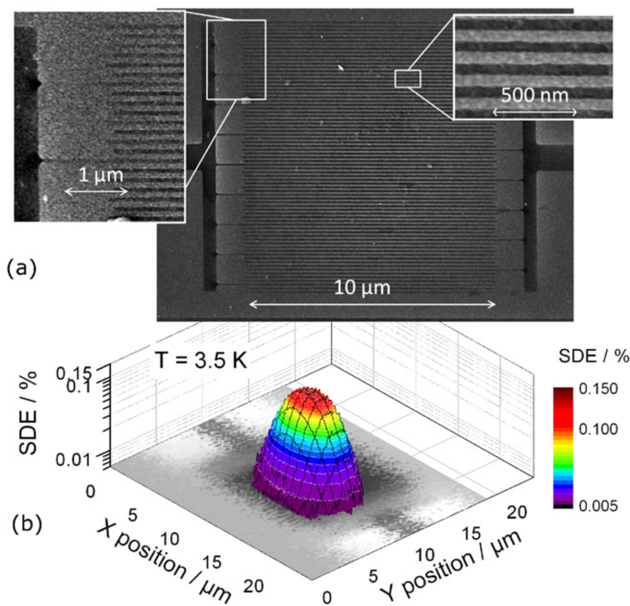

Figure 2. (a) SEM image of a parallel wire LN SNSPD. Varying definition quality is highlighted in the left-hand inset. (b) SNSPD response to illumination over the device area at $\lambda = 1550$ nm, 1 kHz DCR. System detection efficiency is shown with a log-10 scale on the z axis, while colour varies linearly with SDE. The greyscale plot on the base of the figure is an *in situ* reflection map of the device region.

The critical current, I_c, is defined as the maximum current that can be carried by the device while maintaining a superconducting state. This was measured through current biasing the device and monitoring the voltage drop across it. As the true critical current is approached, dark counts often prematurely latch SNSPDs into the resistive state. Our standard experimental arrangement includes a 50 Ω shunt resistor in parallel with the SNSPD to provide a passive reset of the device if a dark count occurs [31]. This allowed a maximum I_c of 11 μA to be reached at 3.5 K, above which the SNSPD remained resistive. I_c improved to 13 μA when cooled to 2.5 K in a different closed cycle refrigerator, discussed later.

The single photon response is measured as a function of position over the device area as shown in figure 2(b). With 1 kHz DCR a peak system detection efficiency (SDE) of 0.15% at $\lambda = 1550$ nm is reached in the device region. However, this decreases over the device area, including some regions (e.g. y position > 12.5 μm) where there is little photoresponse. It should be noted that the device response region ($\sim$5.2 × 3.1 μm FWHM in x and y respectively measured across the peak) is much larger than the measurement resolution.

Close examination of device SEM images reveals that e-beam exposure, resist development or etching parameters have not yet been fully optimized for the LN substrate, leading to non-uniform fabrication results over the large device area. An example is shown in the left inset of figure 2(a). It is likely that variable nanowire dimensions cause the SDE to vary, while fabrication defects may allow current to bypass part of the device area.

Further characterization of the devices at different wavelengths was performed through front side fibre coupling of the SNSPD [19]. A cleaved single mode fibre was mounted in a ferrule and aligned to the device at room temperature. This allowed device response to be studied in a more compact, colder, closed cycle refrigerator at 2.5 K. At this lower temperature an improved I_c of 13 μA was achieved. Single photon response was demonstrated with $\lambda = 830$, 1310 and 1550 nm as shown in figures 3(a) and (b). Measurements were performed with a pulsed laser diode, pulse width $\sim$5 ns, at a repetition rate of 1 MHz. The SDE was calculated as the photon counts after subtraction of the dark counts divided by the photon flux, 1 MHz for figure 3(a) (one photon per pulse incident). The SDE at 1550 nm with 1 kHz DCR ($I/I_c = 0.92$) is comparable to that observed in figure 2(b). The lower temperature gives improved device performance, balanced out by the lower coupling efficiency to the best responding device region. However, increased SDE of $\sim$1% is observed at 830 and 1310 nm at kHz DCR due to the higher photon energy, giving increased probability of hotspot formation. At all three wavelengths SDE increases rapidly at higher bias (higher DCR), reaching $\sim$10% at $I/I_c = 0.98$ with 100 kHz DCR for $\lambda = 830$ nm. In combination with the wavelength dependence of the device response, this suggests that the registering probability (the probability of an output pulse when a photon is absorbed by the nanowire) is low due to a lack of nanowire film or fabrication uniformity limiting the current density in the detector [29], and decreasing the probability of stable hotspot formation and a complete cascade process.

At 1550 nm the FWHM jitter of this SNSPD is 250 ps (figure 3(c)). Studies have shown that nanowire detectors with non-uniform films or lithography have large jitter due to varying hotspot resistance, and therefore pulse shape, over the device area [28]. Low signal to noise ratio of the output pulse also contributed to jitter in this device. A uniform, high film quality, detector on LN may have comparable jitter to detectors on other materials. We found that a detector fabricated from a thicker ($\sim$12 nm) NbN film on LN (right-hand arrow in figure 1(a)) had a uniform optical response over the device region and exhibited 80 ps FWHM jitter. However, low SDE ($\sim$0.003% at 1550 nm, 1 kHz DCR) was exhibited as a result of the low registering probability associated with the thicker film [32, 33].

The 12 nm thick film device with uniform optical response exhibits a Gaussian jitter distribution while the non-uniformly responding 8 nm thick film device is seen to have a non-Gaussian tail extending on the order of nanoseconds. This phenomenon is observed in cascade detectors when a hotspot forms in one wire but the parallel wires fail to cascade immediately [25, 27]. Instead the cascade occurs some time after the initial hotspot formation (for example on occurrence of a dark count), or the detector relaxes back into the fully superconducting state. However, in uniform detectors this tail disappears at high bias when the probability of cascade becomes much closer to unity [34].

Studying the timing properties and efficiency dependence on device bias and photon flux for avalanche or 'SNAP' type detectors yields important information about the operation of

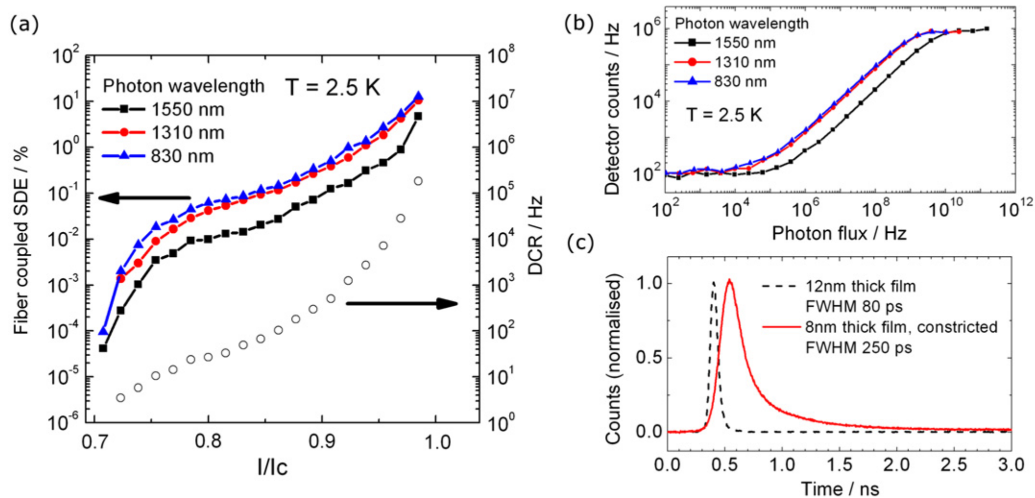

Figure 3. Device characteristics of a fibre coupled LN SNSPD at wavelengths of 830, 1310 and 1550 nm shown in blue (triangle), red (circles) and black (squares), respectively measured at 2.5 K. (a) System detection efficiency (SDE) and dark count rate (DCR, open circles) versus device bias. (b) Single photon detection response to varying photon flux, saturating at the 1 MHz repetition rate of the source. The device is biased at I/I_c ~0.85 with ~100 Hz DCR. (c) Timing jitter of LN SNSPDs.

this variant of the standard meander SNSPD design. This has been studied in detail elsewhere [25, 27, 34]. However, it is important to consider some aspects of the mode of device operation here. It should be possible to trigger true single photon detectors with one photon in isolation. However, an avalanche type detector can also operate in an 'arm and trigger' mode, where the full cascade only occurs due to multiphoton events. It may be that two photons are incident at once, are absorbed into different parallel nanowires, driving both resistive, and cause the device to cascade. Alternatively, one photon arrives driving one nanowire resistive (the 'arm' event) but cascade does not occur until another photon arrives at a later time driving a second nanowire resistive, causing a large enough current redistribution to also drive the remaining nanowires resistive (the 'trigger' event) .

A naïve model assuming perfect current redistribution in a uniform detector with four parallel nanowires suggests that a full avalanche will occur in the detector at a bias $I > 0.75I_c$, defined as the avalanche current, I_{av}. In this scenario the current redistributed from one nanowire to the remaining three is sufficient to drive them resistive. More careful consideration of the dynamics suggests some variation of I_{av} from this simple model [27, 30]. However, it is notable that in figure 3(a) device efficiency and dark counts drop dramatically at this bias, reaching zero below $I = 0.7I_c$ ($< I_{av}$) as the avalanche does not occur.

At higher bias ($I = 0.85I_c > I_{av}$) figure 3(b) shows detector counts scaling linearly with photon flux, describing SDE to be independent of intensity. This characteristic is suggested as an indicator of biasing above the true avalanche SNAP current [27], where true single photon detection occurs. At low bias ($I < I_{av}$), linearity of SDE dependence on photon flux was lost and the device was likely in an arm and trigger regime. However, due to the 1 μs delay between subsequent source pulses, allowing the detector to recover before another photon arrived, it is believed that this regime was improbable; hence the dramatic drop off in SDE at low bias.

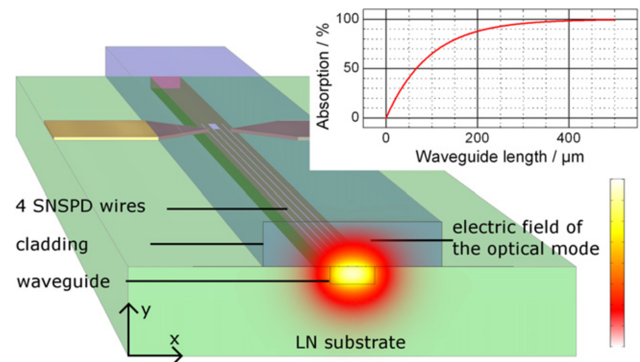

Figure 4. Waveguide integrated SNSPD on a LN waveguide. A simulation of the resultant TE optical mode is shown (the colour scale shows the normalized electric field magnitude, E_x) with evanescent field overlapping the nanowires. Inset: simulated photon absorption into the SNSPD versus waveguide/detector length for the architecture described.

When photons are incident on the detector perpendicular to the surface, the majority of the light is either transmitted or reflected. Under 25% of the optical power is absorbed in the NbN nanowires as the interaction length is limited to the film thickness (calculated through the solution of Fresnel equations at $\lambda = 1550$ nm, with NbN $n \sim 4.2 + 6.5i$). If a waveguide geometry is used, as shown in figure 4, the SNSPD is within the evanescent field of the guided mode. In this simulation a waveguide fabricated through proton exchange (hydrogen absorption) is approximated as a rectangular cross sectioned region of the substrate with dimensions of 5 μm width and 2 μm depth with an increased refractive index ($n = 2.2$, $\Delta n = 0.01$) as compared with the unpatterned substrate. The SNSPD is designed as four wires (8 nm thick by 100 nm wide) running along the length of the waveguide, connected either in series or parallel. An index matched cladding is added on top of the detector and waveguide to allow the waveguide mode to extend vertically over the SNSPD.

Absorption efficiency is controlled by two factors, the strength of the evanescent field overlap with the nanowires and the interaction length. In figure 4 the stable transverse electric (TE) like mode (E_x) of a waveguide created through proton exchange is simulated using a finite element modelling package to solve Maxwell's equations for the guided modes. Due to the contrast between the refractive index of LN ($n \sim 2.2$) and NbN ($n \sim 4.2 + 6.5i$) at 1550 nm wavelength the coupling between the waveguide and detector is not as strong as in Si or GaAs [11, 12]. However, 80% of the light is absorbed in a waveguide length of 150 μm, a total nanowire length less than that of the detector shown in this paper. Increased coupling may be achievable with careful mode engineering.

In this paper we have reported the first meander SNSPD realized on an important substrate, LN, suitable for on-chip integration with high speed quantum optic circuits. Device characteristics show reasonable performance (∼0.15% SDE at 1550 nm with 1 kHz DCR). The substrate temperature for film growth was limited to 200 °C to be compatible with LN waveguides and the film thickness was relatively thick, 8 nm. Lithographic processing was not fully optimized.

NbN is by no means the only superconducting material available for these devices: recently SNSPDs have been demonstrated in NbTiN [18, 19], a-W–Si [35] and Nb–Si [36]. As these materials are amorphous, they are compatible with a wide range of substrates without the need for heated deposition. We are therefore optimistic that, based on our initial result here, nanowire performance on LN can be significantly improved in future allowing SNSPDs to be integrated with complete LN waveguide circuits.

Acknowledgments

The authors would like to thank P Jiang for supplying materials and D Bonneau, M Lobino, M Thompson, J O'Brien for useful discussions. The authors acknowledge funding from the UK Engineering and Physical Sciences Research Council and from NCCR QSIT. RHH also acknowledges a Royal Society University Research Fellowship. WJ gratefully acknowledges a scholarship from the China Scholarship Council (CSC).

References

[1] Nielsen M A and Chuang I L 2010 *Quantum computation and quantum information* (Cambridge: Cambridge University Press)
[2] Hadfield R H 2009 *Nature Photon.* **3** 696–705
[3] Dauler E A, Kerman A J, Robinson B S, Yang J K W, Voronov B, Goltsman G, Hamilton S A and Berggren K K 2009 *J. Mod. Optic.* **56** 364–73
[4] Natarajan C M, Tanner M G and Hadfield R H 2012 *Supercond. Sci. Technol.* **25** 063001
[5] Lobino M *et al* 2011 *Appl. Phys. Lett.* **99** 081110
[6] Xiong C *et al* 2011 *Appl. Phys. Lett.* **98** 051101
[7] Zhang Q, Xie X, Takesue H, Nam S W, Langrock C, Fejer M M and Yamamoto Y 2007 *Opt. Express* **15** 10288–93
[8] Bonneau D, Lobino M, Jiang P, Natarajan C M, Tanner M G, Hadfield R H, Dorenbos S N, Zwiller V, Thompson M G and O'Brien J L 2012 *Phys. Rev. Lett.* **108** 053601
[9] Natarajan C M, Peruzzo A, Miki S, Sasaki M, Wang Z, Baek B, Nam S, Hadfield R H and O'Brien J L 2010 *Appl. Phys. Lett.* **96** 211101
[10] Cavalier P, Villegier J-C, Feautrier P, Constancias C and Morand A 2011 *AIP Adv.* **1** 042120
[11] Pernice W, Schuck C, Minaeva O, Li M, Goltsman G N, Sergienko A V and Tang H X 2011 arXiv:1108.5299v1
[12] Sprengers J P *et al* 2011 *Appl. Phys. Lett.* **99** 181110
[13] Wooten E L *et al* 2000 *IEEE J. Sel. Top. Quant.* **6** 69–82
[14] Miki S, Fujiwara M, Sasaki M, Baek B, Miller A J, Hadfield R H, Nam S W and Wang Z 2008 *Appl. Phys. Lett.* **92** 061116
[15] Marsili F, Bitauld D, Fiore A, Gaggero A, Mattioli F, Leoni R, Benkahoul M and Levy F 2008 *Opt. Express* **16** 3191–6
[16] Gol'tsman G N, Okunev O, Chulkova G, Lipatov A, Semenov A, Smirnov K, Voronov B, Dzardanov A, Williams C and Sobolewski R 2001 *Appl. Phys. Lett.* **79** 705–7
[17] Semenov A *et al* 2009 *Phys. Rev.* B **80** 054510
[18] Dorenbos S N, Reiger E M, Perinetti U, Zwiller V, Zijlstra T and Klapwijk T M 2008 *Appl. Phys. Lett.* **93** 131101
[19] Tanner M G *et al* 2010 *Appl. Phys. Lett.* **96** 221109
[20] Gaggero A *et al* 2010 *Appl. Phys. Lett.* **97** 151108
[21] Osellame R, Lobino M, Chiodo N, Marangoni M, Cerullo G, Ramponi R, Bookey H T, Thomson R R, Psaila N D and Kar A K 2007 *Appl. Phys. Lett.* **90** 241107
[22] Miki S, Fujiwara M, Sasaki M and Wang Z 2007 *IEEE Trans. Appl. Supercond.* **17** 285–8
[23] Il'in K, Siegel M, Engel A, Bartolf H, Schilling A, Semenov A and Huebers H W 2008 *J. Low Temp. Phys.* **151** 585–90
[24] Marsili F, Gaggero A, Li L H, Surrente A, Leoni R, Levy F and Fiore A 2009 *Supercond. Sci. Technol.* **22** 095013
[25] Ejrnaes M *et al* 2009 *Appl. Phys. Lett.* **95** 132503
[26] Ejrnaes M, Cristiano R, Quaranta O, Pagano S, Gaggero A, Mattioli F, Leoni R, Voronov B and Gol'tsman G 2007 *Appl. Phys. Lett.* **91** 262509
[27] Marsili F, Najafi F, Dauler E, Bellei F, Hu X, Csete M, Molnar R J and Berggren K K 2011 *Nano. Lett.* **11** 2048–53
[28] O'Connor J A, Tanner M G, Natarajan C M, Buller G S, Warburton R J, Miki S, Wang Z, Nam S W and Hadfield R H 2011 *Appl. Phys. Lett.* **98** 201116
[29] Kerman A J, Dauler E A, Yang J K W, Rosfjord K M, Anant V, Berggren K K, Gol'tsman G N and Voronov B M 2007 *Appl. Phys. Lett.* **90** 101110
[30] Marsili F, Najafi F, Herder C and Berggren K K 2011 *Appl. Phys. Lett.* **98** 093507
[31] Hadfield R H, Miller A J, Nam S W, Kautz R L and Schwall R E 2005 *Appl. Phys. Lett.* **87** 203505
[32] Verevkin A *et al* 2004 *J. Mod. Opt.* **51** 1447–58
[33] Hofherr M, Rall D, Ilin K, Siegel M, Semenov A, Hubers H W and Gippius N A 2010 *J. Appl. Phys.* **108** 014507
[34] Heath R M, Tanner M G, O'Connor J A, Natarajan C M, Warburton R J, Alvarez L S E, Jiang W, Barber Z H and Hadfield R H 2011 *Single Photon Workshop* (Germany: PTB Braunschweig)
[35] Baek B, Lita A E, Verma V and Nam S W 2011 *Appl. Phys. Lett.* **98** 251105
[36] Dorenbos S N, Forn-Diaz P, Fuse T, Verbruggen A H, Zijlstra T, Klapwijk T M and Zwiller V 2011 *Appl. Phys. Lett.* **98** 251102